A mathematical model to describe hinge crack failure of a sheet ice reinforced ridge beam

Lau, M.

Publisher's version / Version de l'éditeur:
https://doi.org/10.4224/8895803
Contractor Report (National Research Council of Canada. Institute for Marine Dynamics); no. CR-1991-10, 1991

National Research Council Canada
Conseil national de recherches Canada
Institute for Ocean Technology
Institut des technologies océaniques

CR-1991-10

Contractor Report

A Mathematical Model to Describe Hinge Crack Failure of a Sheet Ice Reinforced Ridge Beam

Michael Lau

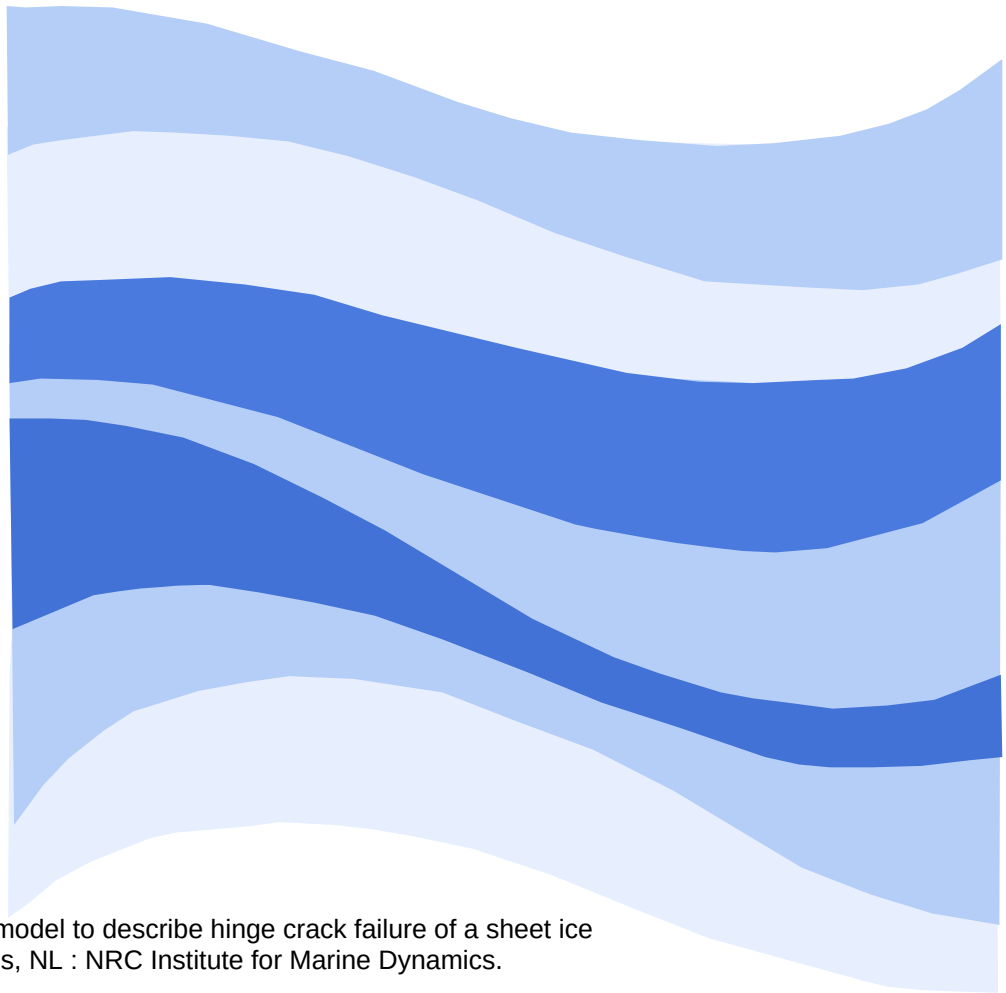

Lau, M., 1991. A mathematical model to describe hinge crack failure of a sheet ice reinforced ridge beam. St. John's, NL : NRC Institute for Marine Dynamics. Contractor Report, CR-1991-10.

Canada

A MATHEMATICAL MODEL TO DESCRIBE HINGE CRACK FAILURE OF A SHEET ICE REINFORCED RIDGE BEAM

Submitted to: National Research Council Canada, Institute for Marine Dynamics

Submitted by: NORDCO Limited

Ref. No.: 175-90G

Date: June, 1991

DOCUMENTATION PAGE

REPORT NUMBER CR-1991-10	NRC REPORT NUMBER -	DATE August 1991
REPORT SECURITY CLASSIFICATION Unclassified		DISTRIBUTION Unlimited

TITLE

A MATHEMATICAL MODEL TO DESCRIBE HINGE CRACK FAILURE OF A SHEET ICE REINFORCED RIDGE BEAM

AUTHOR(S)

Michael Lau

CORPORATE AUTHOR(S)/PERFORMING AGENCY(S)

NORDCO Limited

PUBLICATION

-

SPONSORING AGENCY(S)

Institute for Marine Dynamics
National Research Council Canada

IMD PROJECT NUMBER 292	NRC FILE NUMBER 7819		
KEY WORDS: cones, ridges, mathematical model	PAGES 16	FIGS. 13	TABLES 7

SUMMARY:

A procedure to calculate vertical force on a downward breaking cone encountering a ridge in level ice is presented. The procedure takes into account the stiffening and strengthening contributions of the ice sheet to the ridge beam. Calculated forces are compared with results of model tests.

ADDRESS: National Research Council
Institute for Marine Dynamics
P. O. Box 12093, Station 'A'
St. John's, NF
A1B 3T5

TABLE OF CONTENTS

	Page
LIST OF TABLES	i
LIST OF FIGURES	ii
LIST OF SYMBOLS	iii
ABSTRACT	v
ACKNOWLEDGEMENTS	vi
1.0 INTRODUCTION	1
2.0 MODEL DESCRIPTION	2
2.1 Behaviour of a Sheet Ice Reinforced Ridge Beam: Hinge Crack Formation	2
2.2 Analytical Model	3
2.2.1 Effect of Ice Sheet Spring Stiffness	4
2.2.2 Effective Flange	5
2.2.3 Hinge Crack Formulae for Infinitely Long Composite Beam	6
2.2.4 Transformed Section Method	7
2.2.5 Stress Distributions at Failure	7
2.3 Procedure for Calculating Hinge Crack Forces	8
2.4 Comparison with Model Test Results	10
2.5 Non-Dimensional Analysis	12
3.0 CONCLUSIONS	15
4.0 REFERENCES	16

ABSTRACT

This report presents a mathematical procedure to calculate vertical hinge crack load on a downward breaking conical structure when it encounters a multi-year pressure ridges frozen into a level ice field.

The purpose is to provide realistic analytical estimates for comparison with experimental data obtained in a previous model test in which substantial difference in mechanical properties of the ridges and the surrounding ice sheet was encountered.

The model is based on Hetenyi's theory of an elastic beam on an elastic foundation. The difference in mechanical properties of the ridges and the surrounding ice sheet was incorporated into the analysis by treating the ridge/ice system as a composite beam.

In addition to presenting the mathematical procedure, the results of the previous test program are compared with the analytical estimates as a means of validating the procedure.

A method to calculate the non-dimensional force and the non-dimensional width utilizing the model is also developed. Good agreement is found between the model predictions and the measurements.

ACKNOWLEDGMENTS

This project was funded by the National Research Council of Canada through the Institute for Marine Dynamics (IMD). The author sincerely thanks Dr. F.M. Williams of the institute for her valuable input throughout this study.

LIST OF TABLES

TABLES

Summary of Model Ice Properties (Ridge-Ice System)	Table 1
Summary the Analytical Predictions (Sheet Detached)	Table 2
Summary the Analytical Predictions (Onset of Hinge Crack)	Table 3
Summary the Analytical Predictions (Final Failure)	Table 4
Comparison of Measured and Predicted Forces	Table 5
Summary of Non-Dimensional Analysis (Sheet Detached)	Table 6
Summary of Non-Dimensional Analysis (Peak Load)	Table 7

LIST OF FIGURES

FIGURES

Stress Distribution at the Onset of Hinge Crack	Fig. 1
Stress Distribution at the Completion of Hinge Crack	Fig. 2
Deflection of a Semi-Infinite Ice Strip	Fig. 3
Non-Uniform Distribution of Tensile Stress, σ_{st}, and The Corresponding Effective Width, b_{eff}	Fig. 4
Transformed Section of a Ridge Sheet Composite	Fig. 5
Cross-Sectional Profile of the Model Ridge	Fig. 6
CONE10 - Vertical Ridge Breaking Forces vs. Ridge Width, WLD = 1.28 m and H = 75.8 m	Fig. 7
CONE10 - Vertical Ridge Breaking Forces vs. Ridge Width, WLD = 1.48 m and H = 75.8 m	Fig. 8
CONE12 - Vertical Ridge Breaking Forces vs. Ridge Width, WLD = 1.08 m and H = 106.5 m	Fig. 9
CONE12 - Vertical Ridge Breaking Forces vs. Ridge Width, WLD = 1.28 m and H = 106.5 m	Fig. 10
CONE12 - Vertical Ridge Breaking Forces vs. Ridge Width, WLD = 1.48 m and H = 106.5 m	Fig. 11
CONE10 - Non-Dimensional Force vs. Non-Dimensional Ridge Width	Fig. 12
CONE12 - Non-Dimensional Force vs. Non-Dimensional Ridge Width	Fig. 13

LIST OF SYMBOLS

A_s	Cross-sectional area of ice flange
E_R	Elastic modulus of ice ridge
E_s	Elastic modulus of ice sheet
F_V	Measured vertical ridge breaking force
H	Thickness of ice ridge
H_e	Equivalent thickness of transformed rectangular beam
I_R	Moment of inertia of ice ridge
M	Moment
NF_V	Non-dimensional vertical ridge breaking force
NW_R	Non-dimensional ridge width
P_{NS}	Predicted maximum ridge force calculated with ice sheet detached
P_{HC}	Predicted ridge force for the onset of hinge crack
P_{FL}	Predicted ridge force for full development of hinge crack
P_{PL}	Predicted maximum ridge force calculated with sheet attached
WLD	Waterline diameter of cone
W_R	Ridge width
V	Vertical force
b_{eff}	Effective width of ice flange
d	Hinge crack location measured from the tip of the cantilever ridge beam
g	Gravitational acceleration
h	Thickness of ice sheet
k	Foundation modulus
k^*	Adjusted foundation modulus accounted for spring stiffness of surrounding ice sheet
l_R	Characteristic length of ice ridge
l_s	Characteristic length of ice sheet
n	Modulus ratio
ρ_w	Density of doped water
v	Poisson's ratio for ice
y	Distance from neutral axis to failure surface
y_r	$y/(0.5\ H_e)$

z	Location of neutral axis measured from the bottom fibre of ridge
σ_C	Compressive strength of ice ridge
σ_F	Flexural strength of ice ridge
σ_f	Flexural strength of ice sheet
σ_{gov}	Governing strength at failure
σ_{rt}	Tensile stress at top fibre of ridge
σ_{rb}	Compressive stress at bottom fibre of ridge
σ_{st}	Tensile stress at top fibre of attached ice sheet

1.0 INTRODUCTION

In a recent model test (Lau, 1990) conducted by NORDCO Limited with a 45 degree conical structure in multi-year pressure ridges frozen into a level ice field, a phenomenon in which the surrounding ice sheet acting as a tensile reinforcement to the ridge beam was observed. The reinforcement tended to slow down the crack development and increased the loading capacity of the ridge substantially. This phenomenon is not satisfactorily explained by existing analytical models.

In the present study, a mathematical procedure is developed to calculate the ice ridge failure forces associated with the formation of the hinge crack in which the reinforcement phenomenon occurs. The purpose is to provide realistic analytical estimates for comparison with experimental data obtained in the fore-mentioned test program.

In this report, the mathematical model is described in Section 2. In Section 3 the accuracy of the model is assessed by comparing the analytical estimates with the test data. Conclusions are contained in Section 4.

2.0 MODEL DESCRIPTION

Previous model tests on ridge/cone interactions showed that many modes of failure are possible depending on the geometric and material properties of the ice and cone. The presence of the ice sheet further complicates the problem.

If the ridge-ice sheet interface is strong and the ridge flexural strength is low, the hinge crack may occur before the ridge and ice sheet separate. In such situations, the attached ice sheet essentially acts as tensile reinforcement to the ridge beam.

The present procedure only deals with the behaviour of a sheet ice reinforced ridge beam under bending. Only hinge crack failure is described although the procedure can be modified to include center crack failure.

2.1 Behaviour of a Sheet Ice Reinforced Ridge Beam: Hinge Crack Formation

When a vertical concentrated load acting on the tip of a semi-infinite floating cantilever ridge beam is gradually increased from zero to that magnitude which will cause the beam to fail, a hinge crack appears approximately at a distance,

$$d = \frac{\pi}{4} l_R \qquad (1)$$

from the point of loading, where l_R is the characteristic length of the ridge beam.

Several different stages of behaviour can be clearly distinguished at the hinge crack location. At low loads, as long as the maximum tension stress in the ridge is smaller than the flexural strength, the entire ridge

is effective in resisting stress. In addition, the attached ice sheet, deforming the same amount as the adjacent ridge, is also subjected to tension stress.

When the load is further increased, the tension strength of the ridge ice is soon reached, and at this stage tension cracks develop. The distribution of stresses in the ridge and the ice sheet over the depth of the section is shown in Figure 1. If the failure strain of the sheet ice is substantially greater than the failure strain of the ridge beam; the crack will be confined to the top surface of the ridge beam without penetrating into the ice sheet. As the loading increases the crack penetrates downward toward the level of the neutral plane, which in turn shifts downward with progressive cracking, with the redistribution of tensile stress to the ice sheet. This tends to slow down the crack development, thus allowing a number of hinge cracks to develop adjacent to the first hinge crack.

Eventually, the load carrying capacity of the ridge beam is reached. Failure can be initiated either by tensile failure of the ice sheet at the top surface or by crushing of the ridge at the bottom surface. The corresponding stress distributions are given in Figure 2.

If crushing of ridge occurs, higher failure load may result due to plastic deformation of the crushed area of the ridge.

2.2 Analytical Model

The theory adopted in this study to calculate the forces experienced at the various stages of hinge crack formation is based on Hetenyi's theory of an elastic beam on an elastic foundation (Hetenyi, 1946). The difference in mechanical properties of the ridge and the surrounding ice sheet is incorporated into the procedure by treating the ridge/ice system as a composite beam.

The attached ice sheet affects the loading of the ridge beam in 2 major ways:

1. It modifies the deflection curve of the ridge by increasing the spring stiffness of the foundation.

2. It effectively acts with the ridge beam and contributes to its strength in bending through the increase of its section modulus.

2.2.1 Effect of Ice Sheet Spring Stiffness

As the ridge slides down the cone surface, the level ice sheet connected to the ridge is forced to follow the deflection of the ridge beam. The extra load necessary to deflect the ice has the effect of making the foundation "appear" to be stiffer than if the ridge were considered by itself.

The stiffening effect of the ice sheet on the ridge deflection can be determined by treating the ice sheet as a series of infinitesimal beams with the imposed conditions that the deflection of the ice sheet at the junction with the ridge be equal to the deflection of the ridge and that the slope in the direction perpendicular to the ridge be zero. (See Figure 3.) The additional force needed to deflect the ice sheet during ridge deflection may then be treated as additional spring force equally distributed along the edge of the ridge beam which increases the foundation modulus by

$$2\ (2)^{0.5}\ \rho_w g\ l_s.$$

Thus, the effect of ice sheet spring stiffness can be accounted for by replacing the foundation modulus, $k = \rho_w g W_R$, by an adjusted foundation modulus

$$k^* = \rho_w g\ (W_R + 2\ (2)^{0.5}\ l_s) \qquad (2)$$

where W_R = width of ridge at waterline

l_s = characteristic length of ice sheet as given by

$$l_s = \left(\frac{E_s h^3}{12\,(1 - v^2)\,p_w g} \right)^{1/4} \qquad (3)$$

E_s = elastic modulus of ice sheet

v = Poisson's ratio for ice

h = ice sheet thickness

The derivation of Equation 2 is given by Hysing and Bach-Gansmo (1981).

2.2.2 Effective Flange

Due to shear strain in the plane of the ice sheet, longitudinal bending stress is not constant across the ice sheet. The intensity of the extreme fibre tensile stress, which is maximum over the ridge beam, decreases non-linearly as the distance from the beam increases as shown in Figure 4.

For practical purposes, the concept of an effective flange width, b_{eff}, is used to simplify the more complex lateral distribution effect for an infinitely wide ice sheet. The effective width of each flange is

$$b_{eff} = \frac{(2)^{0.5}\, l_s}{(1 - v^2)} \qquad (4)$$

In deriving this effective width, the objective is to select an equivalent uniform stress, which is assumed to act over a reduced width, b_{eff}, which produces the same resultant force in the ice sheet as the actual stress, which varies over the full width of the ice sheet.

The theory involved in the determination of the effective width is briefly discussed by Wang and Salmon (1973).

2.2.3 Hinge Crack Formulae for Infinitely Long Composite Beam

The load causing hinge crack of an infinite elastic beam on an elastic foundation can be estimated by the following simple beam formulae:

$$P_V = 6.2 \frac{\sigma_{gov} I_R}{y l_R} \quad (5)$$

where

P_V = vertical load causing hinge crack

I_R = moment of inertia of pressure ridge with or without ice sheet attached

y = distance to outer fibre at which failure occurs, from neutral axis

l_R = characteristic length of the ridge

$$l_R = \left(\frac{4 E_R I_R}{k^*} \right)^{1/4} \quad (6)$$

E_R = elastic modulus of ridge

σ_{gov} = flexural strength or compressive strength of the ridge, depending on the stress distribution at failure

This equation holds for a homogeneous beam when a constant value of elastic modulus applies across a section. However, it cannot be used directly to solve the composite beam problem as in the present case when the elastic modulus, E_S, of the ice sheet is significantly different from the elastic modulus, E_R, of the ridge.

To complicate the problem, the stress distribution (thus the failure load) associated with failure depends on the failure strengths of both the ice sheet and the ridge.

2.2.4 Transformed Section Method

To analyse this type of beam the composite section is transformed into a single material. This transformed area concept makes it possible to replace a composite member with an equivalent member of homogeneous elastic material to which the basic strength of materials relationships apply.

In the present analysis the effective flange of ice sheet calculated using equation 4 are transformed into an equivalent area, nA_S, of ridge ice located at the level of the ice sheet where A_S is the original cross-sectional area of the ice flange. n is called modular ratio defined as

$$n = \frac{E_S}{E_R} \qquad (7)$$

where E_S and E_R are the elastic moduli for the sheet and ridge ice respectively. The original and the transformed sections are shown in Figure 5. The equivalent flexural strength of the ice sheet in the transformed section is equal to σ_f/n.

Once the transformed section has been obtained, the analysis of bending proceeds as though the beam were composed of homogeneous ridge ice and the simple beam equation 5 can then be applied to the transformed section.

2.2.5 Stress Distribution at Failure

Figure 1 shows the cross-section and stress distribution at the onset of the hinge crack. In the model test the failure strain of the sheet ice , defined as σ_f/E_S, was typically 3 times greater than the failure strain,

σ_F/E_R, of the ridge beam, thus, the crack was confined to the top surface of the ridge beam without penetrating into the ice sheet and the failure is determined by the tensile strength at the top fibre of the ridge.

Figure 2 shows the cross-sections and stress distributions at the completion of the hinge crack. At this time, the top of the ridge has already failed due to tension. The final failure will then be determined by either the equivalent sheet ice strength, σ_f/n, or the compressive ridge ice strength, σ_C, whichever is exceeded first.

After the stress distribution at various stages of the hinge crack development is known, the corresponding moment of inertia I_R and the distance y associated with the failure of the transformed section can be calculated and equation 5 can then be applied directly.

2.3 Procedure for Calculating Hinge Crack Forces

The procedure for calculating loading at various stages of the hinge crack development is given as follow:

STEP 1 Calculate the adjusted foundation modulus,

$$k^* = p_w g \ (W_R + 2 \ (2)^{0.5} \ l_s) \tag{2}$$

where

$$l_s = \left(\frac{E_s h^3}{12 \ (1 - v^2) \ p_w g} \right)^{1/4} \tag{3}$$

STEP 2 Calculate effective flange,

$$b_{eff} = \frac{(2)^{0.5} \ l_s}{(1 - v^2)} \tag{4}$$

of the surrounding ice sheet.

STEP 3 Calculate the modulus ratio,

$$n = \frac{E_S}{E_R} \qquad (7)$$

and transform the effective flanges of the ice sheet into an equivalent area, nA_S, of the ridge ice to obtained the transformed section as shown in Figure 5. The equivalent flexural strength of ice sheet equals to σ_f/n.

STEP 4 Calculate the moment of inertia, I_R, of the transformed section. The moments of inertia about the neutral axis of the transformed section can be found using the parallel axis theorem.

STEP 5 Calculate the characteristic length, l_R,

$$l_R = \left(\frac{4\, E_R\, I_R}{k^*} \right)^{1/4} \qquad (6)$$

of the composite ridge beam.

STEP 6 Load at the onset of hinge crack:
Assuming the stress distribution as shown in Figure 1, calculate the distance, y, from the neutral axis and the moment of inertia, I_R, of the uncracked section.
The neutral axis of this transformed section is at its centroid.
Simple beam formulae:

$$P_V = 6.2\, \frac{\sigma_{gov}\, I_R}{y\, l_R} \qquad (5)$$

can then be applied with $\sigma_{gov} = \sigma_F$.

STEP 7 Load at the completion of hinge crack:

To compute the failure load of the cracked beam, the procedure described in step 6 can still be used. Two possible stress distributions are given in Figure 2. The stress distributions is depended either on the equivalent flexural strength, σ_f/n, of ice sheet or compressive strength, σ_C, of ridge whichever is exceeded first. One need only to identify the appropriate stress distribution. Trial and error method can be used to identify the correct stress distribution. Once the appropriate stress distribution is identified, the computation in Step 6 can then followed.

2.4 Comparison With Model Test Results

Load estimates calculated from the described procedure are compared with test values obtained from the two tests in the previous study (Lau, 1990) to assess the accuracy of the model.

Ridge beams with widths ranging from 0.17 to 1.00 m were tested. The first test, test CONE10, was performed at waterlines of 1.28 and 1.48 m and a ridge thickness of 75.8 mm. The second test, test CONE12, was performed at waterlines of 1.08, 1.28, and 1.48 m and ridge thickness of 106.5 mm. The ridges were embedded in a level ice sheet approximately 36 mm thick.

A typical vertical cross-section of the model ridges is shown in Figure 6a. The structure consists of two distinct materials. A strong rectangular cross-sectional area surrounded by a layer of weaker sheet ice resulting in a trapezoidal shape.

For the sake of simplicity the ridges are idealized as beams of rectangular cross-section with ice sheet attached as shown in Figure 6b.

The properties of the ridge ice and the surrounding ice sheet are summarized in Table 1.

Load Estimates were calculated for the following cases:

1. Failure of the ridge beam with the effect of the ice sheet ignored.

2. Failure of the ridge/sheet composite beam: onset of the hinge crack

3. Failure of the ridge/sheet composite beam: completion of the hinge crack

Summaries of the analytical predictions for the above 3 cases are given in Tables 2 to 4.

For the test data, the forces due to ridge failure alone are obtained by subtracting the ice clearing force from the total force, because by the time the ridge failed against the cone, the broken ice of the preceding ice sheet still covered a significant portion of the front half of the cone surface. The clearing force has been determined by use of the elastic model of Kim and Kotras (1973).

The estimates are plotted together with the measured values against ridge width in Figures 7 to 11 for different ridge thickness and cone waterlines. Three curves are shown in each figure. One represents the failure due to the ridge beam alone without the contribution of the surrounding ice sheet. The other two represents the load due to the sheet/ridge beam combination: one for the onset of the hinge crack and the other one for the completion of the hinge crack.

Several conclusions can be drawn from the comparisons:

1. The contribution from the ice sheet to peak load is significant in the present test conditions. Thus, a simple analysis in which the ice sheet is ignored severely underestimates the peak load.

2. By including the attached ice sheet in the analysis, the estimates are substantially improved. The agreement between the theory and the experiment is remarkable. For test CONE10, the differences between the predicted and experimental values are very low, while, for test CONE12, the theory slightly underestimates the forces.

3. The model predicts no increase of ice force after the onset of hinge crack beyond certain ridge width and thickness. This reflects the fact that with a relatively weak ice sheet, the increase in governing strength is not large enough to compensate for the decrease in section modulus of the cracked beam at failure. (See equation 5) For the failure loads, only the maximum values of Figures 7 to 11 are of interest. Thus the maximum values of case 2 and 3 should be regarded as peak forces.

Ratios of the measured and the predicted force values for each case are also given in Table 5.

2.5 Non-Dimensional Analysis

A method of calculating the non-dimensional ridge breaking force and ridge width based on equation 5 is given in the following section. These factors allow comparison with data between the two tests.

To simplify the derivation, the ridge beam is transformed into an equivalent rectangular beam with the same moment of inertia I_R and ridge width W_R, thus

$$I_R = \frac{1}{12} W_R H_e^3 \qquad (8)$$

where H_e = the equivalent thickness of the transformed rectangular beam

Substituting equation 8 into equation 5, a simple relationship of the force and width in non-dimensional form can be deduced:

$$0.97 \frac{F_V * y_r}{\sigma_{gov} H_e^2} = \frac{W_R}{l_R} \qquad (9)$$

where

$$y_r = \frac{y}{0.5 H_e} \qquad (10)$$

The factor, $0.97\ y_r/(\sigma_{gov} H_e^2)$, is used to non-dimensionalize the vertical force, and the factor, $1/l_R$, is used to non-dimensionalize the ridge width.

Calculations were performed for the peak loads corresponding to the following two cases:

1. Failure of the ridge beam
2. Failure of the ridge/sheet composite beam

A summary of the non-dimensional analysis with the data from both tests are given in Tables 6 and 7.

Figures 12 and 13 show the non-dimensional forces, NF_V, versus non-dimensional width, NW_R, for test CONE10 and test CONE12 respectively. The

parameters of the regression lines for the two cases are shown in the following table.

	CASE 1			CASE 2		
Test	slope	intercept	rms	slope	intercept	rms
CONE10	0.911	0.264	0.033	1.011	-0.022	0.037
CONE12	1.409	0.165	0.033	1.416	-0.033	0.033

Examination of the regression lines shows that the force-width relationships for the two ridge thicknesses are different, reflecting the need for further investigation.

3.0 CONCLUSIONS

A mathematical procedure to calculate vertical hinge crack load on a downward breaking conical structure when it encounters a multi-year pressure ridge frozen into a level ice sheet has been developed and presented.

Calculated values of the loads causing flexural failure of a sheet ice reinforced ridge beam comply very well with corresponding model test results.

A method to calculate the non-dimensional forces and the non-dimensional width based on the procedure is also developed. Good agreement is found between the model predictions and the measurements.

The comparison also suggests that the contribution from the ice sheet to peak load is significant in the present test condition. Thus, a simple analysis in which the ice sheet is ignored severely underestimates the peak load.

4.0 REFERENCES

1. HETENYI, M. "Beam on Elastic Foundations," The University of Michigan Press, Ann Arbor, Michigan, 1946.

2. KIM, J.K., and KOTRAS, T.V. "Mathematical Model to Describe the Behaviour of a Moving Ice Field Encountering a Conical Structure", APOA Project 57, Revised Report prepared for APOA by Arctec Canada Ltd., Montreal, Vol. 1, 1973.

3. HYSING, T. and BACH-GANSMO, O. "Loads on Offshore Structures Due to Multi-Year Ridges", Marine Structures and Ships in Ice, Report No. 81-07, 1981.

4. LAU, M. "Model Test Investigation of Level and Multi-Year Ridge Ice Forces on Downward Breaking Conical Structures", IMD/NRC Report CR-1990-08, March 1990.

5. WANG, C.K. and SALMON, C.G. Reinforced Concrete Design, 2nd Edition, Intext Press Inc., New York, pp.142-144, 1973.

Table 1

SUMMARY OF MODEL ICE PROPERTIES
(RIDGE ICE SYSTEM)

Run (#)	σ_F (kPa)	σ_C (kPa)	E_R (MPa)	l_R[1] (cm)	W_R (cm)	σ_f (kPa)	E_S (MPa)	k^*[1] (kPa)	l_S (cm)	b_{eff}[2] (cm)	n
Test Name: CONE10 WLD: 1.28 m H: 75.8 mm h: 36.3 mm											
1	88.5	198	139	81.8	17.0	35.6	23.5	10.6	32.2	51.2	0.169
2	87.8	197	138	89.7	31.4	34.8	23.0	12.0	32.0	50.9	0.166
3	87.2	195	137	95.0	48.0	34.2	22.6	13.5	31.9	50.7	0.164
5	85.9	192	135	97.2	58.4	33.0	21.8	14.5	31.6	50.3	0.161
6	82.9	186	130	99.7	77.1	30.2	19.9	16.1	30.9	49.2	0.153
7	82.2	184	129	100.9	87.6	29.6	19.5	17.1	30.7	48.9	0.151
Test Name: CONE10 WLD: 1.48 m H: 75.8 mm h: 36.3 mm											
9	80.1	180	126	81.5	19.1	27.9	18.4	10.3	30.3	48.2	0.146
10	79.7	179	125	89.6	36.1	27.6	18.2	11.9	30.2	48.1	0.145
11	79.1	177	125	92.0	43.8	27.1	17.9	12.6	30.1	47.8	0.144
12	78.8	176	124	96.6	64.7	26.8	17.7	14.7	30.0	47.7	0.143
13	78.0	175	123	98.0	73.7	24.5	16.2	15.4	29.3	46.7	0.132
14	77.7	174	122	101.2	100.0	24.3	16.0	17.9	29.3	46.6	0.131
Test Name: CONE12 WLD: 1.48 m H: 106.5 mm h: 36.8 mm											
1	117.2	230	309	144.2	43.9	40.4	35.9	14.3	36.2	57.6	0.116
2	115.8	227	305	150.3	59.8	39.6	35.2	15.8	36.0	57.3	0.116
3	115.4	226	304	156.6	82.7	39.3	35.0	18.1	35.9	57.2	0.115
Test Name: CONE12 WLD: 1.28 m H: 106.5 mm h: 36.8 mm											
5	110.9	217	292	129.5	23.8	36.7	32.7	12.1	35.3	56.2	0.112
6	110.2	216	290	140.8	40.7	36.3	32.3	13.8	35.2	56.0	0.111
7	110.2	216	290	148.5	59.0	36.1	32.1	15.5	35.2	56.0	0.111
8	109.1	214	287	154.4	81.3	35.8	31.9	17.7	35.1	55.9	0.111
Test Name: CONE12 WLD: 1.08 m H: 106.5 mm h: 36.8 mm											
10	107.2	210	282	130.3	25.7	33.6	29.9	12.1	34.6	55.0	0.106
11	106.4	209	280	142.0	45.2	33.2	29.5	14.0	34.4	54.8	0.105
12	105.7	207	278	147.1	58.6	32.9	29.3	15.3	34.4	54.7	0.105
13	105.3	206	277	153.3	81.1	32.6	29.0	17.5	34.3	54.6	0.105

NOTE:
1. l_R and k^* are calculated with the ice sheet attached.
2. b_{eff} is for one flange only.

Table 2

SUMMARY OF THE ANALYTICAL PREDICTIONS: SHEET DETACHED

Run (#)	y^2 (cm)	σ_{gov}[1] (KPa)	l_R (cm)	I_{R_4} (cm^4)	P_{NS} (N)
Test Name: CONE10 WLD: 1.28 m H: 75.8 mm					
1	3.79	88.5	119.9	0.062	75
2	3.79	87.8	119.6	0.114	137
3	3.79	87.2	119.4	0.174	208
5	3.79	85.9	119.0	0.212	250
6	3.79	82.9	117.9	0.280	322
7	3.79	82.2	117.7	0.318	363
Test Name: CONE10 WLD: 1.48 m H: 75.8 mm					
9	3.79	80.1	116.9	0.069	78
10	3.79	79.7	116.8	0.131	146
11	3.79	79.1	116.5	0.159	176
12	3.79	78.8	116.4	0.235	260
13	3.79	78.0	116.1	0.267	294
14	3.79	77.7	116.0	0.363	398
Test Name: CONE12 WLD: 1.48 m H: 106.5 mm					
1	5.32	117.2	188.7	0.442	320
2	5.32	115.8	188.1	0.602	431
3	5.32	115.4	188.0	0.832	595
Test Name: CONE12 WLD: 1.28 m H: 106.5 mm					
5	5.32	110.9	186.1	0.240	166
6	5.32	110.2	185.8	0.410	283
7	5.32	110.2	185.8	0.594	410
8	5.32	109.1	185.4	0.818	561
Test Name: CONE12 WLD: 1.08 m H: 106.5 mm					
10	5.32	107.2	184.6	0.259	175
11	5.32	106.4	184.2	0.455	306
12	5.32	105.7	183.9	0.590	395
13	5.32	105.3	183.7	0.816	545

NOTE:
1. $\sigma_{gov} = \sigma_F$
2. $y = 0.5\ H$

Table 3

SUMMARY OF THE ANALYTICAL PREDICTIONS: ONSET OF HINGE CRACK

Run (#)	z (cm)	y^2 (cm)	σ_{rb} (kPa)	σ_{st} (kPa)	σ_{gov}[1] (kPa)	l_R (cm)	I_R (cm^4)	P_{HC} (N)
				Test Name: CONE10 WLD: 1.28 m H: 75.8 mm				
1	4.44	3.14	124.9	14.92	88.5	81.8	0.085	182
2	4.19	3.39	108.8	14.59	87.8	89.7	0.140	251
3	4.07	3.51	101.2	14.34	87.2	95.0	0.201	326
5	4.02	3.56	97.1	13.83	85.9	97.2	0.239	368
6	3.96	3.62	90.6	12.66	82.9	99.7	0.305	434
7	3.94	3.64	88.8	12.41	82.2	100.9	0.343	476
				Test Name: CONE10 WLD: 1.48 m H: 75.8 mm				
9	4.31	3.27	105.3	11.70	80.1	81.5	0.090	167
10	4.10	3.48	93.8	11.57	79.7	89.6	0.153	243
11	4.05	3.53	90.7	11.36	79.1	92.0	0.181	274
12	3.97	3.61	86.6	11.24	78.8	96.6	0.258	361
13	3.94	3.64	84.2	10.27	78.0	98.0	0.289	391
14	3.90	3.68	82.3	10.19	77.7	101.2	0.384	497
				Test Name: CONE12 WLD: 1.48 m H: 106.5 mm				
1	5.66	4.99	132.9	13.65	117.2	144.2	0.502	507
2	5.57	5.08	127.1	13.38	115.8	150.3	0.662	623
3	5.51	5.14	123.5	13.28	115.4	156.6	0.894	794
				Test Name: CONE12 WLD: 1.28 m H: 106.5 mm				
5	5.86	4.79	135.8	12.40	110.9	129.5	0.292	324
6	5.66	4.99	124.9	12.27	110.2	140.8	0.465	452
7	5.56	5.09	120.4	12.20	110.2	148.5	0.651	588
8	5.50	5.15	116.5	12.10	109.1	154.4	0.876	745
				Test Name: CONE12 WLD: 1.08 m H: 106.5 mm				
10	5.80	4.85	128.1	11.35	107.2	130.3	0.309	324
11	5.61	5.04	118.4	11.22	106.4	142.0	0.507	467
12	5.55	5.10	114.9	11.12	105.7	147.1	0.643	561
13	5.49	5.16	111.9	11.02	105.3	153.3	0.870	717

NOTE: 1. $y = H - z$
2. $\sigma_{gov} = \sigma_F$

Table 4

SUMMARY OF THE ANALYTICAL PREDICTIONS: FINAL FAILURE

Run (#)	Mode[1] (#)	z (cm)	y[1] (cm)	y1[2] (cm)	σ_{rb} (kPa)	σ_{st} (kPa)	σ_{gov}[2] (kPa)	l_R (cm)	I_{R_4} (cm^4)	P_{FL} (N)
				Test Name: CONE10 WLD: 1.28 m H: 75.8 mm						
1	1	4.01	1.79	4.01	198.3	29.7	198.3	81.8	0.066	247
2	2	3.46	1.73	4.12	176.0	34.8	209.4	89.7	0.088	310
3	2	3.16	1.85	4.42	148.8	34.2	207.9	95.0	0.108	333
5	2	3.03	1.91	4.55	136.2	33.0	204.9	97.2	0.118	339
6	2	2.84	1.99	4.74	118.6	30.2	197.6	99.7	0.132	342
7	2	2.78	2.01	4.80	113.3	29.6	196.0	100.9	0.140	351
				Test Name: CONE10 WLD: 1.48 m H: 75.8 mm						
9	1	3.71	1.65	3.71	179.5	27.4	179.5	81.5	0.063	231
10	2	3.23	1.82	4.35	141.2	27.6	190.1	89.6	0.086	260
11	2	3.10	1.88	4.48	130.5	27.1	188.7	92.0	0.094	267
12	2	2.88	1.97	4.70	115.1	26.8	187.8	96.6	0.115	294
13	2	2.77	2.02	4.81	107.2	24.5	186.0	98.0	0.117	287
14	2	2.65	2.07	4.93	99.7	24.3	185.3	101.2	0.139	321
				Test Name: CONE12 WLD: 1.48 m H: 106.5 mm						
1	2	3.99	2.25	6.66	207.7	40.4	346.9	144.2	0.230	514
2	2	3.71	2.34	6.94	183.5	39.6	342.7	150.3	0.260	529
3	2	3.48	2.42	7.17	165.7	39.3	341.3	156.6	0.298	563
				Test Name: CONE12 WLD: 1.28 m H: 106.5 mm						
5	1	4.67	2.38	4.67	217.4	31.2	217.4	129.5	0.176	392
6	2	3.99	2.25	6.66	195.4	36.3	325.9	140.8	0.214	460
7	2	3.67	2.36	6.98	171.7	36.1	325.9	148.5	0.249	485
8	2	3.45	2.43	7.20	154.9	35.8	322.8	154.4	0.287	516
				Test Name: CONE12 WLD: 1.08 m H: 106.5 mm						
10	1	4.44	2.26	4.44	210.2	31.1	210.2	130.3	0.172	387
11	2	3.83	2.30	6.82	176.9	33.2	314.8	142.0	0.213	430
12	2	3.62	2.37	7.03	161.3	32.9	312.8	147.1	0.238	446
13	2	3.41	2.45	7.24	146.4	32.6	311.5	153.3	0.274	476

NOTE:
1. Failure criterion: 1 - compressive failure at the bottom of ridge, 2 - tensile failure at top surface of ice sheet
2. For mode 1: $y = z$, $\sigma_{gov} = \sigma_c$,
   mode 2: $y = H - z$, $\sigma_{gov} = \sigma_f/n$

Table 5

COMPARISON OF MEASURED AND PREDICTED FORCES

Run (#)	W_R (N)	Predicted P_{NS} (N)	Predicted P_{HC} (N)	Predicted P_{FL} (N)	Predicted P_{PL} (N)	F_V[1] (N)	Predicted/Measured P_{NS}/F_V	Predicted/Measured P_{HC}/F_V	Predicted/Measured P_{PL}/F_V
Test Name: CONE10 WLD: 1.28 m H: 75.8 mm									
1	17.0	75	182	247	247	213	0.35	0.85	1.16
2	31.4	137	251	310	310	269	0.51	0.93	1.15
3	48.0	208	326	333	333	345	0.60	0.94	0.97
5	58.4	250	368	339	368	351	0.71	1.05	1.05
6	77.1	322	434	342	434	397	0.81	1.09	1.09
7	87.6	363	476	351	476	454	0.80	1.05	1.05
Test Name: CONE10 WLD: 1.48 m H: 75.8 mm									
9	19.1	78	167	231	231	173	0.45	0.97	1.34
10	36.1	146	243	260	260	251	0.58	0.97	1.04
11	43.7	176	274	267	274	286	0.62	0.96	0.96
12	64.7	260	361	294	361	381	0.68	0.95	0.95
13	73.7	294	391	287	391	414	0.71	0.94	0.94
14	100.0	398	497	321	497	474	0.84	1.05	1.05
Test Name: CONE12 WLD: 1.48 m H: 106.5 mm									
1	43.9	320	507	514	514	717	0.45	0.71	0.72
2	59.8	431	623	529	623	885	0.49	0.70	0.70
3	82.7	595	794	563	794	1005	0.59	0.79	0.79
Test Name: CONE12 WLD: 1.28 m H: 106.5 mm									
5	23.8	166	324	392	392	401	0.41	0.81	0.98
6	40.7	283	452	460	460	653	0.43	0.69	0.70
7	59.0	410	588	485	588	762	0.54	0.77	0.77
8	81.3	561	745	516	745	1043	0.54	0.71	0.71
Test Name: CONE12 WLD: 1.08 m H: 106.5 mm									
10	25.7	175	324	387	387	420	0.42	0.77	0.92
11	45.2	306	467	430	467	628	0.49	0.74	0.74
12	58.6	395	561	446	561	803	0.49	0.70	0.70
13	81.1	545	717	476	717	915	0.60	0.78	0.78

NOTE: 1. Measured maximum ridge breaking force

Table 6

SUMMARY OF NON-DIMENSIONAL ANALYSIS (SHEET DETACHED)

Run (#)	σ_{gov} (kPa)	H (cm)	F_V (N)	NF_V[1]	W_R (cm)	l_R (cm)	NW_R[2]
	Test Name: CONE10 WLD: 1.28 m H: 75.8 mm						
1	88.5	7.58	213	0.405	17.0	119.9	0.142
2	87.8	7.58	269	0.516	31.4	119.6	0.263
3	87.2	7.58	345	0.667	48.0	119.4	0.402
5	85.9	7.58	351	0.689	58.4	119.0	0.491
6	82.9	7.58	397	0.808	77.1	117.9	0.654
7	82.2	7.58	454	0.932	87.6	117.7	0.745
	Test Name: CONE10 WLD: 1.48 m H: 75.8 mm						
9	80.1	7.58	173	0.365	19.1	116.9	0.163
10	79.7	7.58	251	0.532	36.1	116.8	0.309
11	79.1	7.58	286	0.611	43.7	116.5	0.375
12	78.8	7.58	381	0.817	64.7	116.4	0.556
13	78.0	7.58	414	0.897	73.7	116.1	0.635
14	77.7	7.58	474	1.030	100.0	116.0	0.862
	Test Name: CONE12 WLD: 1.48 m H: 106.5 mm						
1	117.2	10.65	717	0.523	43.9	188.7	0.233
2	115.8	10.65	885	0.653	59.8	188.1	0.318
3	115.4	10.65	1005	0.745	82.7	188.0	0.440
	Test Name: CONE12 WLD: 1.28 m H: 106.5 mm						
5	110.9	10.65	401	0.309	23.8	186.1	0.128
6	110.2	10.65	653	0.507	40.7	185.8	0.219
7	110.2	10.65	762	0.592	59.0	185.8	0.318
8	109.1	10.65	1043	0.818	81.3	185.4	0.439
	Test Name: CONE12 WLD: 1.08 m H: 106.5 mm						
10	107.2	10.65	420	0.335	25.7	184.6	0.139
11	106.4	10.65	628	0.505	45.2	184.2	0.245
12	105.7	10.65	803	0.650	58.6	183.9	0.319
13	105.3	10.65	915	0.743	81.1	183.7	0.441

NOTE: 1 The measured forces are non-dimensionalized by multiplying $0.97/(\sigma_{gov} * H^2)$
2 The width is non-dimensionalized by dividing l_R

Table 7

SUMMARY OF NON-DIMENSIONAL ANALYSIS (PEAK LOAD)

Run (#)	y_r	σ_{gov} (kPa)	H_e (cm)	F_V (N)	NF_V[1]	W_R (cm)	l_R (cm)	NW_R[2]
			Test Name: CONE10 WLD: 1.28 m H: 75.8 mm					
1	1.04	198.3	7.75	213	0.179	17.0	81.8	0.208
2	1.18	209.4	6.96	269	0.304	31.4	89.7	0.350
3	1.37	207.9	6.47	345	0.524	48.0	95.0	0.505
5	0.90	85.9	7.89	351	0.574	58.4	97.2	0.601
6	0.93	82.9	7.80	397	0.708	77.1	99.7	0.774
7	0.94	82.2	7.78	454	0.830	87.6	100.9	0.868
			Test Name: CONE10 WLD: 1.48 m H: 75.8 mm					
9	1.01	179.5	7.33	173	0.176	19.1	81.5	0.234
10	1.32	190.1	6.59	251	0.390	36.1	89.6	0.403
11	0.89	79.1	7.92	286	0.499	43.7	92.0	0.476
12	0.92	78.8	7.82	381	0.709	64.7	96.6	0.669
13	0.94	78.0	7.77	414	0.799	73.7	98.0	0.752
14	0.95	77.7	7.72	474	0.945	100.0	101.2	0.988
			Test Name: CONE12 WLD: 1.48 m H: 106.5 mm					
1	1.56	346.9	8.56	717	0.425	43.9	144.2	0.304
2	0.92	115.8	11.00	885	0.566	59.8	150.3	0.398
3	0.94	115.4	10.90	1005	0.670	82.7	156.6	0.528
			Test Name: CONE12 WLD: 1.28 m H: 106.5 mm					
5	0.97	217.4	9.61	401	0.188	23.8	129.5	0.184
6	1.55	325.9	8.57	653	0.411	40.7	140.8	0.289
7	0.93	110.2	10.98	762	0.516	59.0	148.5	0.397
8	0.95	109.1	10.89	1043	0.739	81.3	154.4	0.526
			Test Name: CONE12 WLD: 1.08 m H: 106.5 mm					
10	0.96	210.2	9.29	420	0.215	25.7	130.3	0.197
11	0.91	106.4	11.04	628	0.429	45.2	142.0	0.318
12	0.93	105.7	10.96	803	0.571	58.6	147.1	0.398
13	0.95	105.3	10.88	915	0.676	81.1	153.3	0.529

NOTE: 1 The measured forces are non-dimensionalized by multiplying $0.97*(y_r)/(\sigma_{gov} * H_e^2)$
2 The width is non-dimensionalized by dividing l_R

Figure 1

STRESS DISTRIBUTION AT THE ONSET OF HINGE CRACK

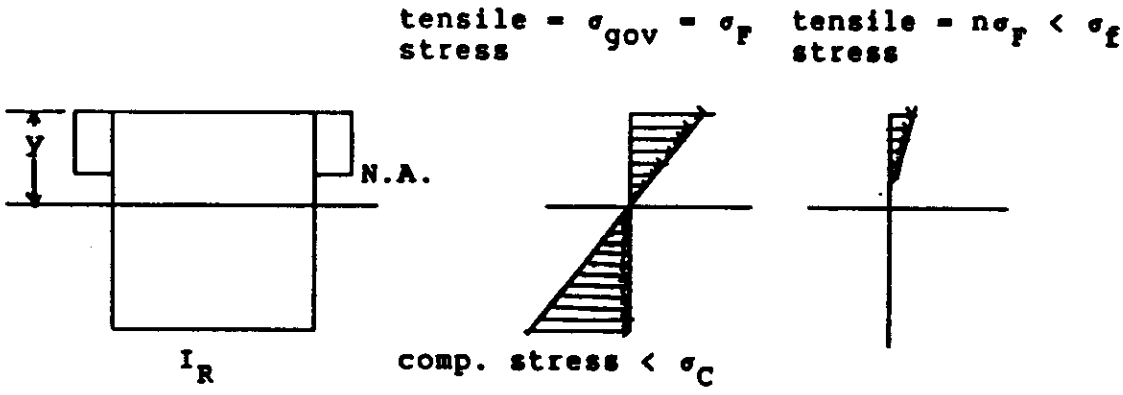

UNCRACKED BEAM SECTION

ICE FLANGES

CROSS SECTION AT FAILURE

STRESS DISTRIBUTION

Figure 2

STRESS DISTRIBUTION AT THE COMPLETION OF HINGE CRACK

A. STRESS DISTRIBUTION AT FINAL FAILURE (TENSILE FAILURE OF SHEET)

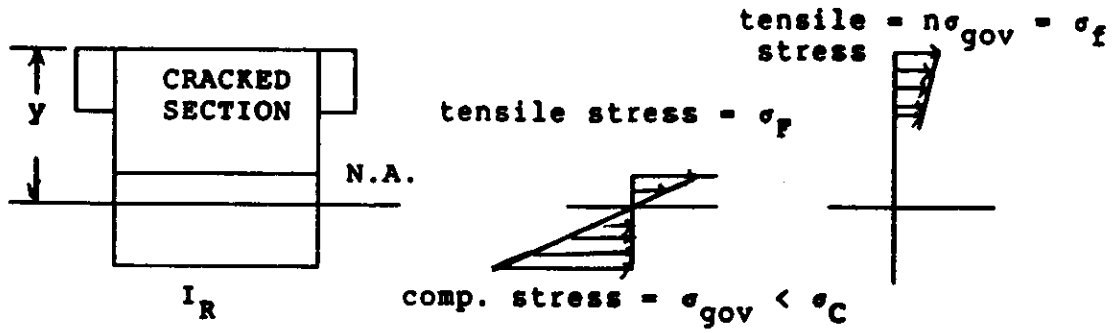

UNCRACKED BEAM SECTION

ICE FLANGES

CROSS SECTION AT FAILURE

STRESS DISTRIBUTION

B. STRESS DISTRIBUTION AT FAILURE (COMPRESSIVE FAILURE OF RIDGE)

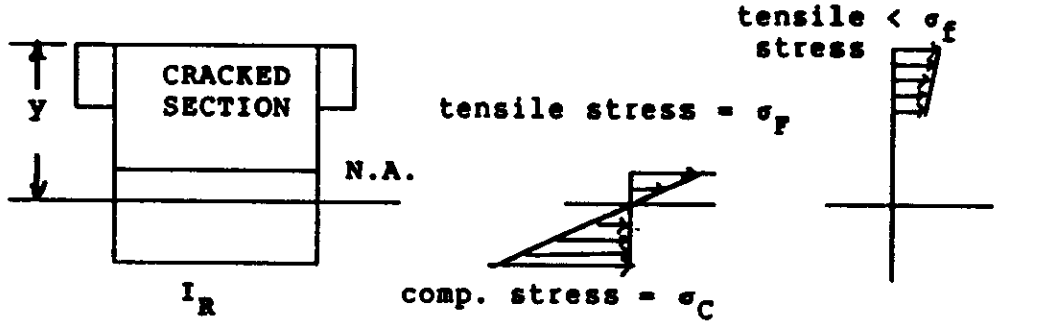

UNCRACKED BEAM SECTION

ICE FLANGES

CROSS SECTION AT FAILURE

STRESS DISTRIBUTION

Figure 3

DEFLECTION OF A SEMI-INFINITE ICE STRIP

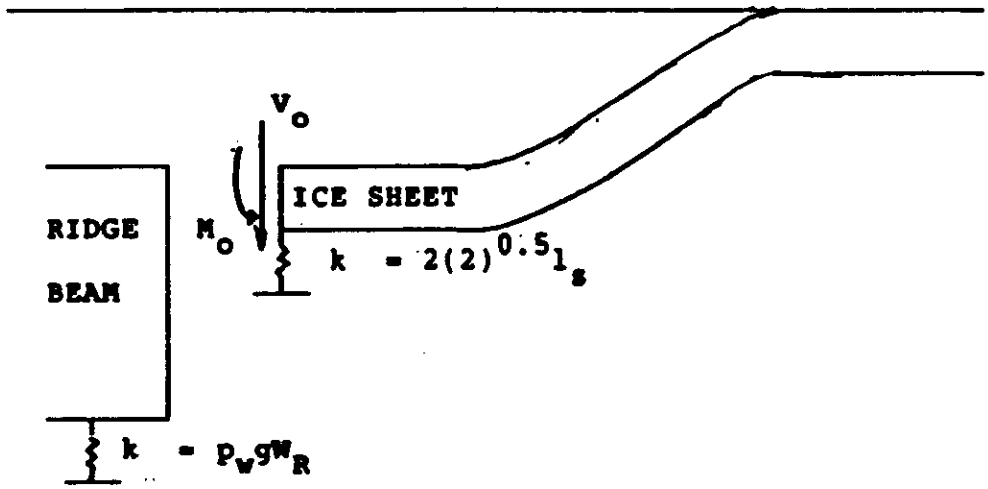

Figure 4

NON-UNIFORM DISTRIBUTION OF TENSILE STRESS, σ_{st}, AND THE CORRESPONDING EFFECTIVE WIDTH, b_{eff}

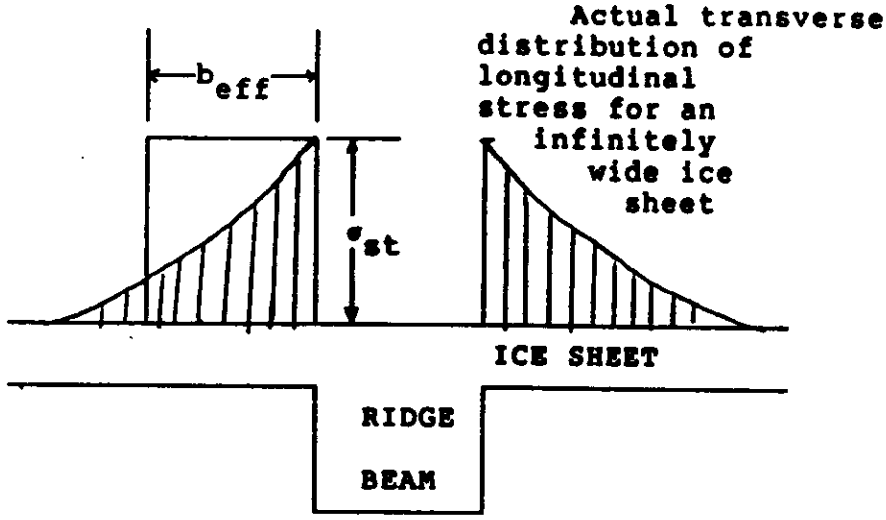

b_{eff} = Equivalent width for uniform stress distribution - for approximately the same effect as the actual distribution

TRANSFORMED SECTION OF A RIDGE SHEET COMPOSITE

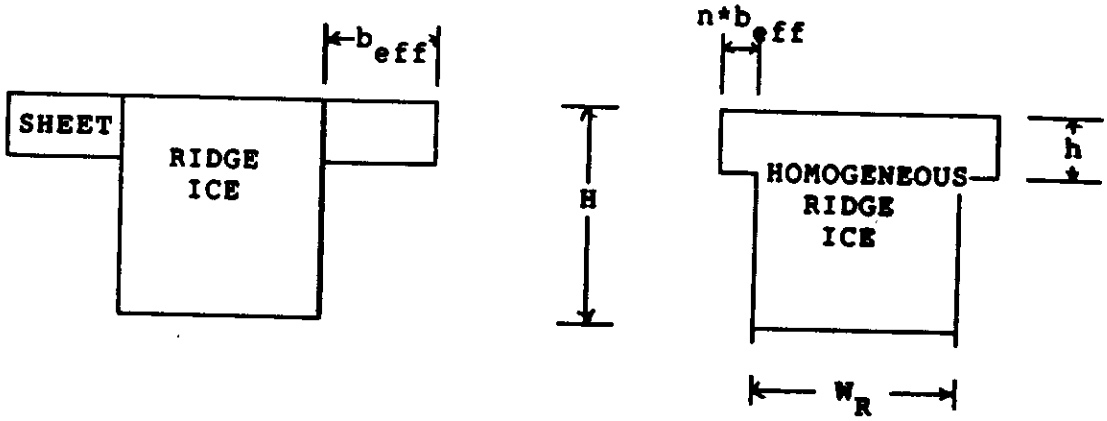

RIDGE SHEET COMPOSITE

TRANSFORMED SECTION

Figure 6

CROSS-SECTIONAL PROFILE OF THE MODEL RIDGE

A) ACTUAL RIDGE CROSS-SECTION

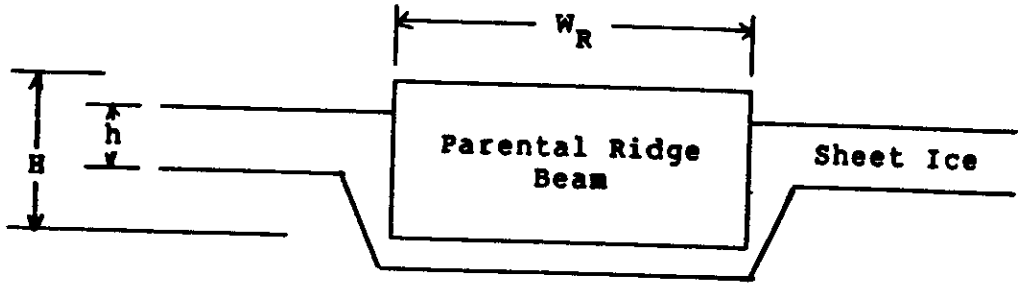

B) IDEALIZED RIDGE CROSS-SECTION

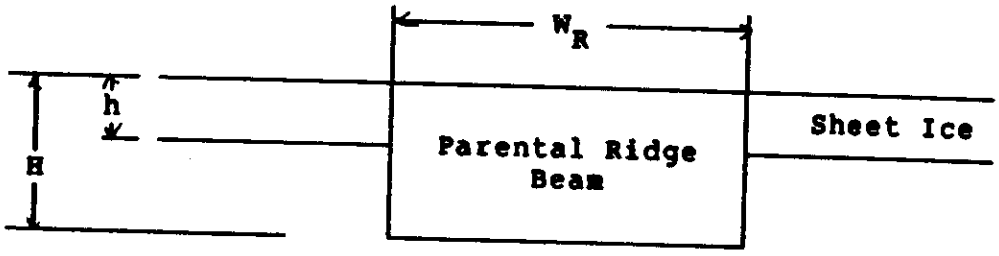

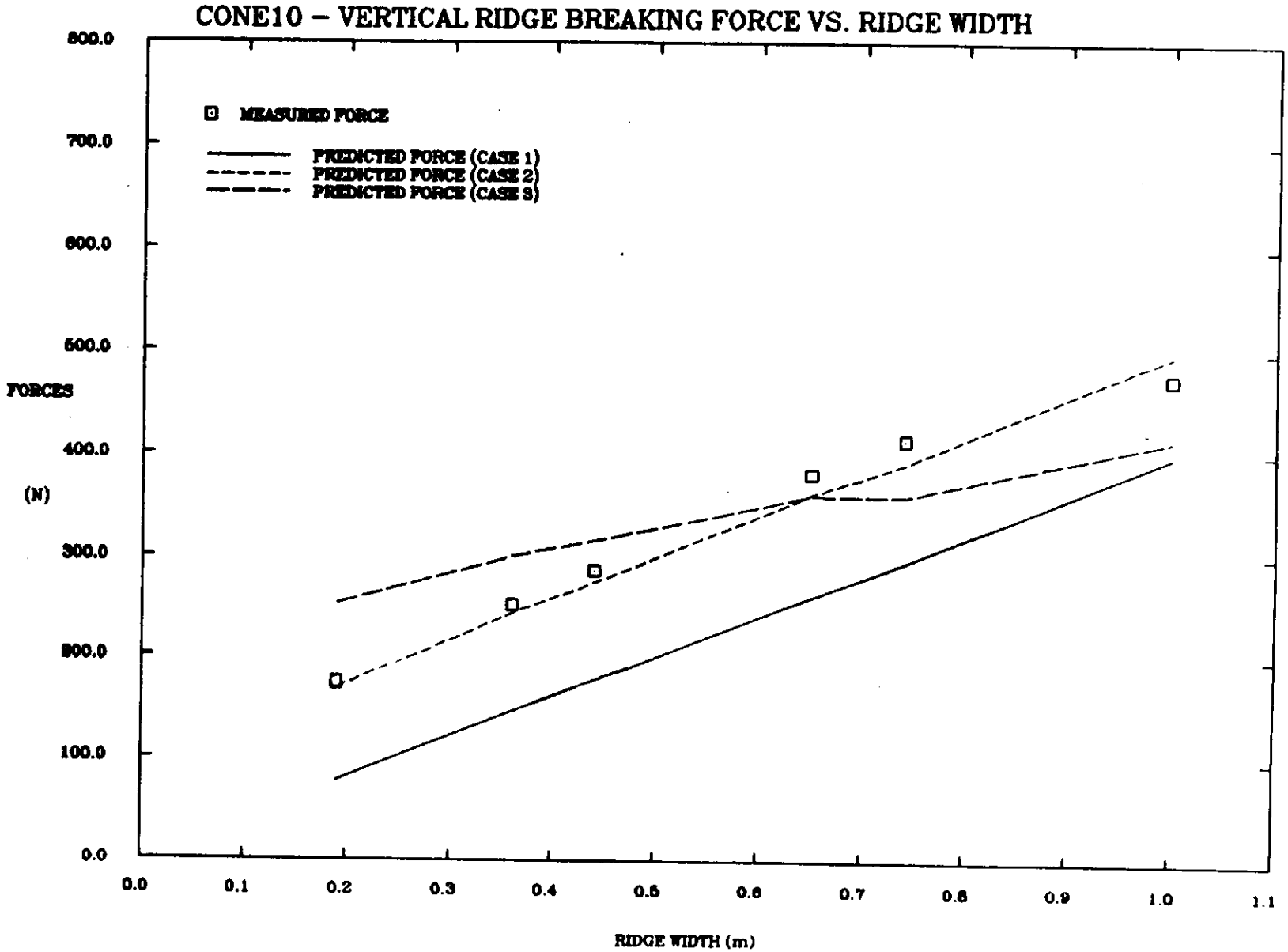

Figure 7

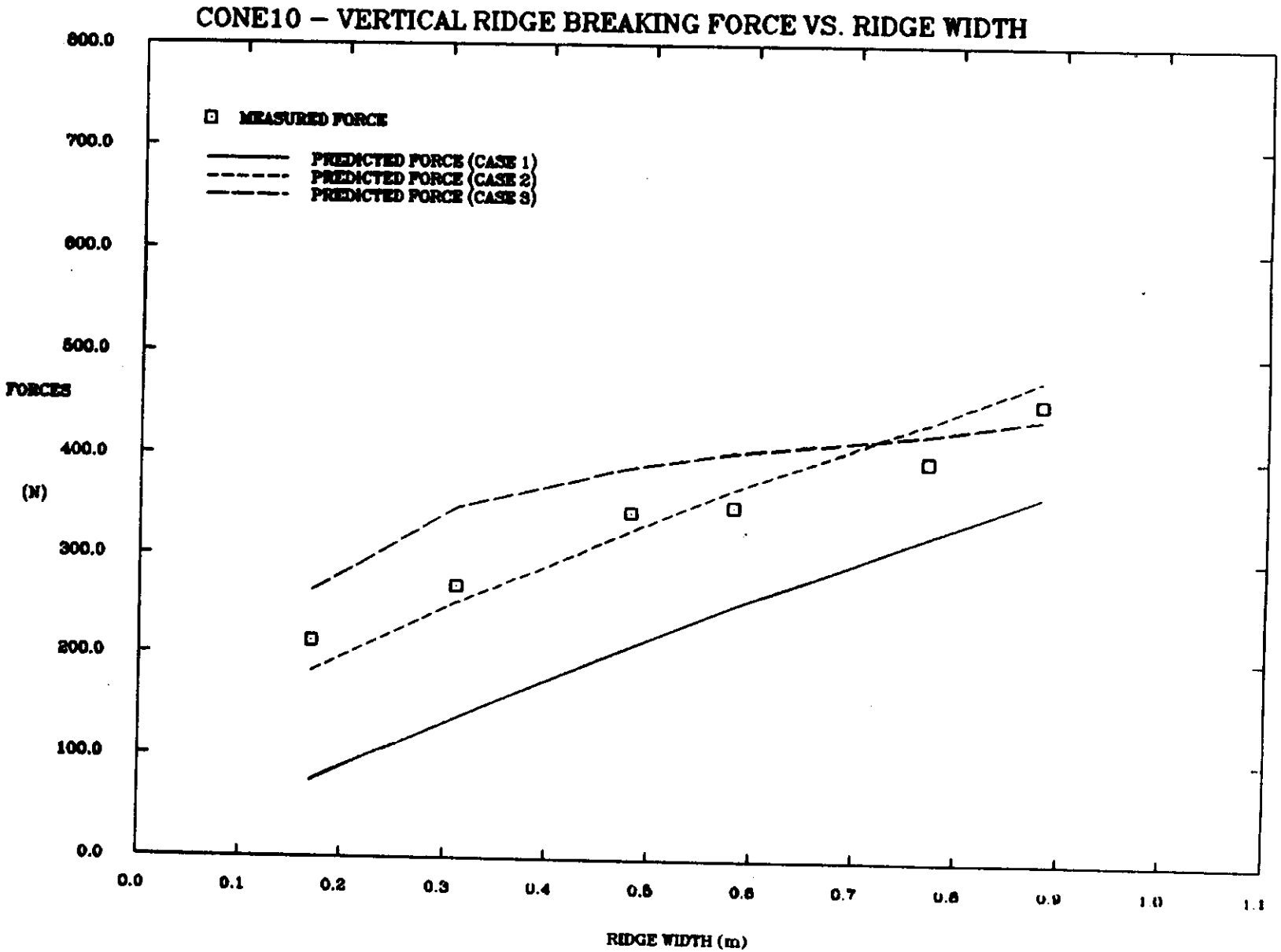

Figure 8

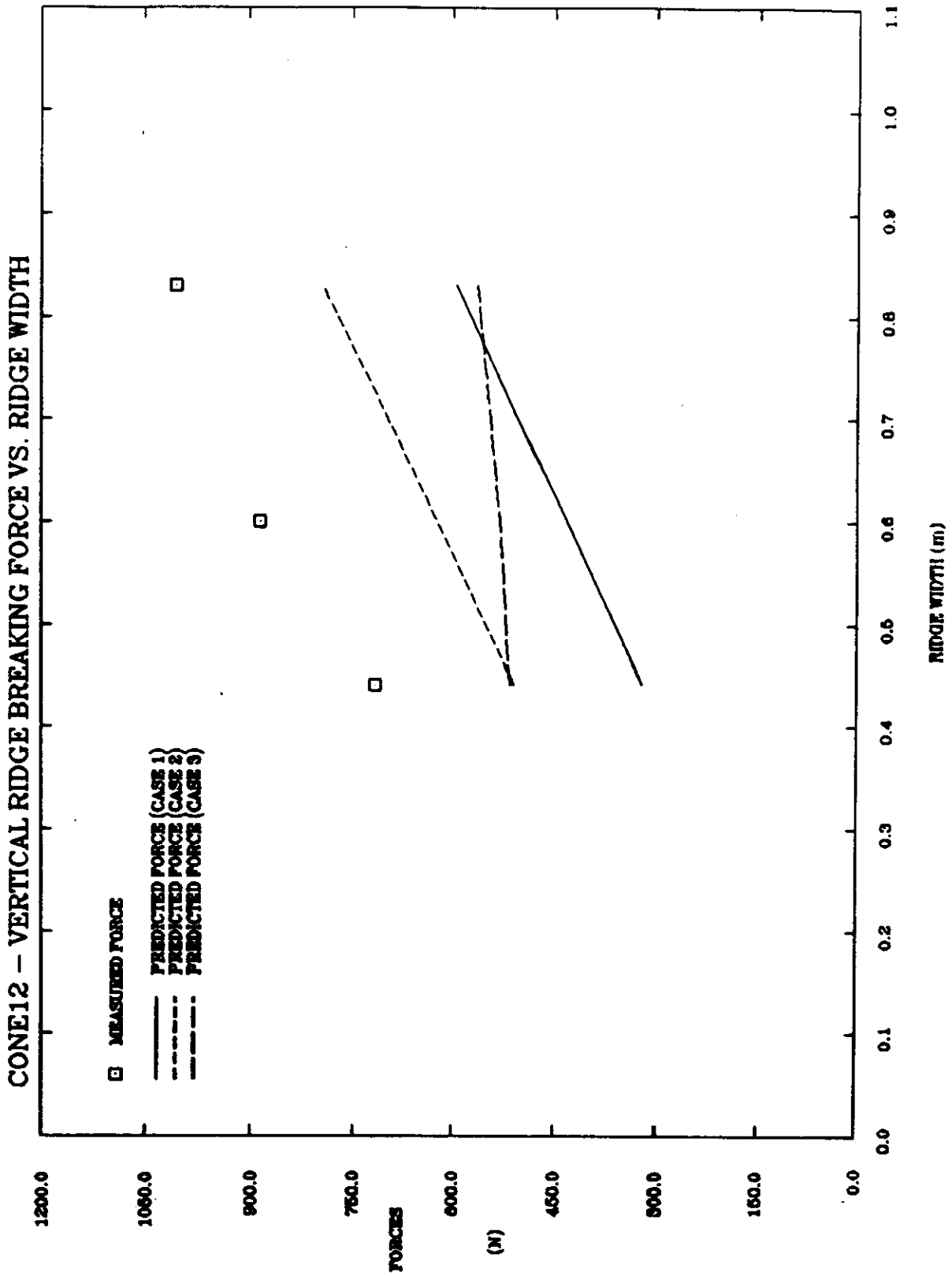
CONE12 – VERTICAL RIDGE BREAKING FORCE VS. RIDGE WIDTH
MEASURED FORCE
PREDICTED FORCE (CASE 1)
PREDICTED FORCE (CASE 2)
PREDICTED FORCE (CASE 3)
FORCES (N)
1200.0
1050.0
900.0
750.0
600.0
450.0
300.0
150.0
0.0
0.0
0.1
0.2
0.3
0.4
0.5
0.6
0.7
0.8
0.9
1.0
1.1
RIDGE WIDTH (m)

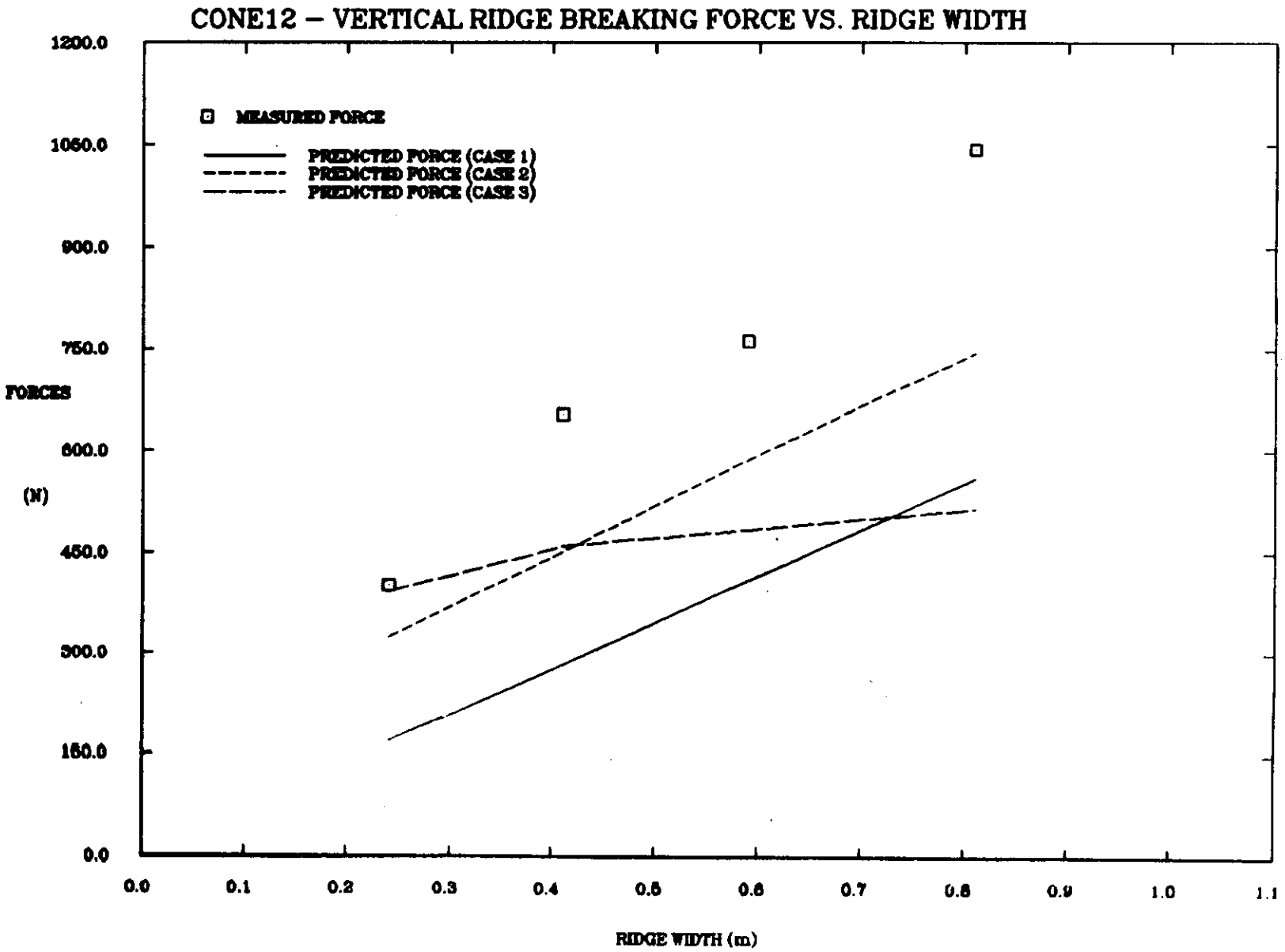

Figure 10

Figure 11

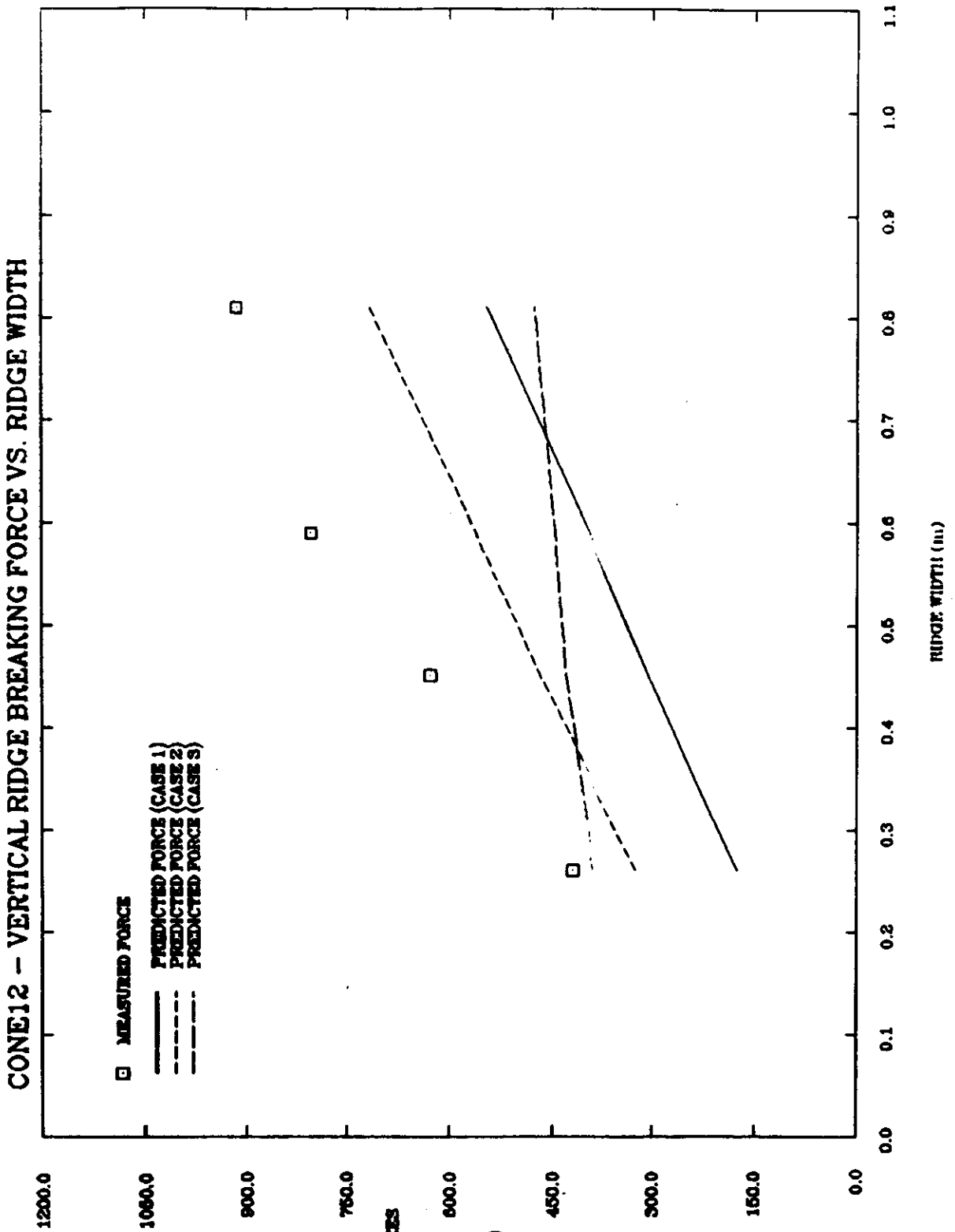
CONE12 – VERTICAL RIDGE BREAKING FORCE VS. RIDGE WIDTH
MEASURED FORCE
PREDICTED FORCE (CASE 1)
PREDICTED FORCE (CASE 2)
PREDICTED FORCE (CASE 3)
FORCES (N)
RIDGE WIDTH (m)
1200.0
1050.0
900.0
750.0
600.0
450.0
300.0
150.0
0.0
0.0
0.1
0.2
0.3
0.4
0.5
0.6
0.7
0.8
0.9
1.0
1.1

Figure 12

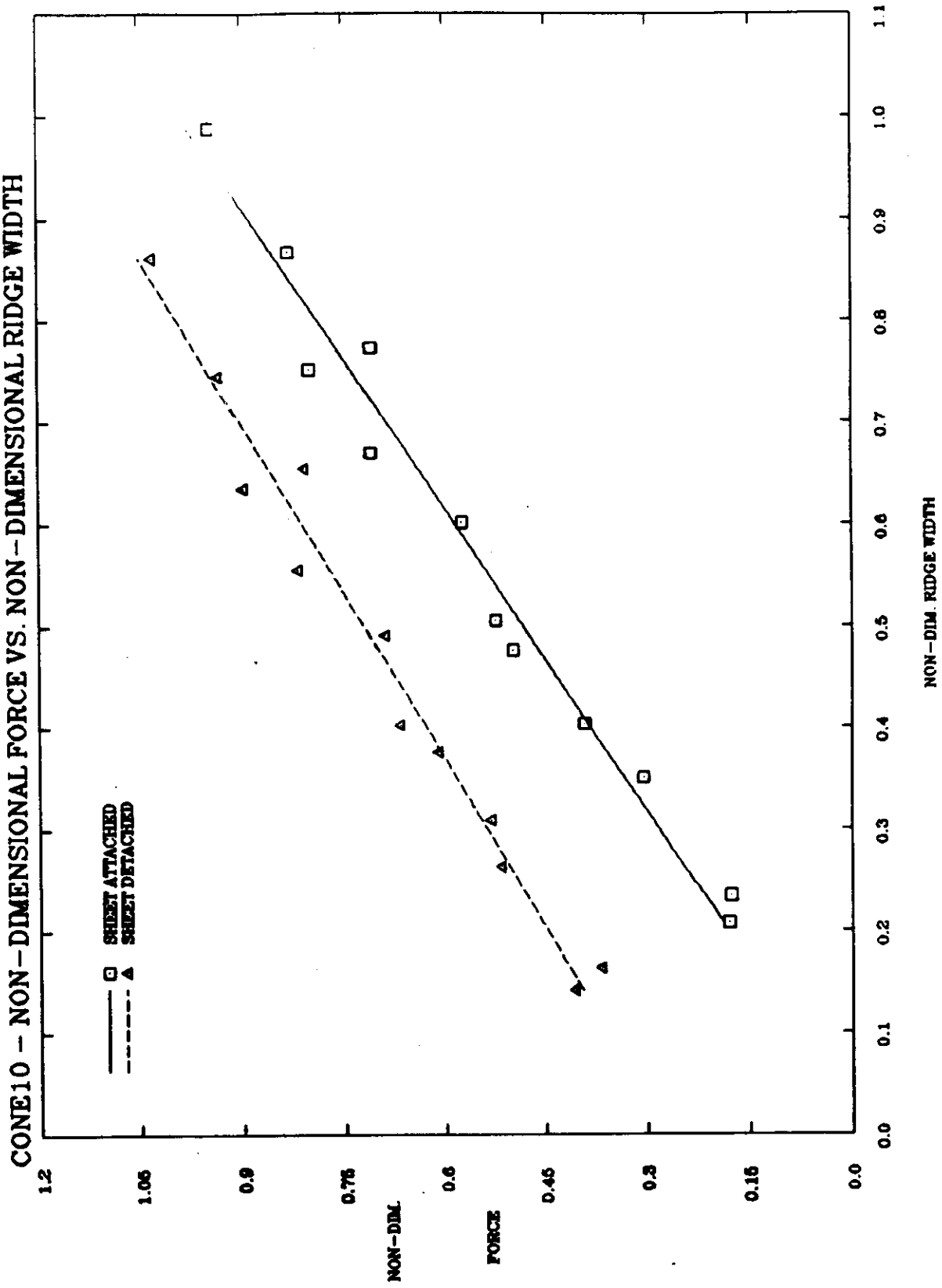
CONE10 – NON–DIMENSIONAL FORCE VS. NON–DIMENSIONAL RIDGE WIDTH
SHEET ATTACHED
SHEET DETACHED
NON–DIM. FORCE
NON–DIM. RIDGE WIDTH
1.2
1.05
0.9
0.75
0.6
0.45
0.3
0.15
0.0
0.0
0.1
0.2
0.3
0.4
0.5
0.6
0.7
0.8
0.9
1.0
1.1

Figure 13

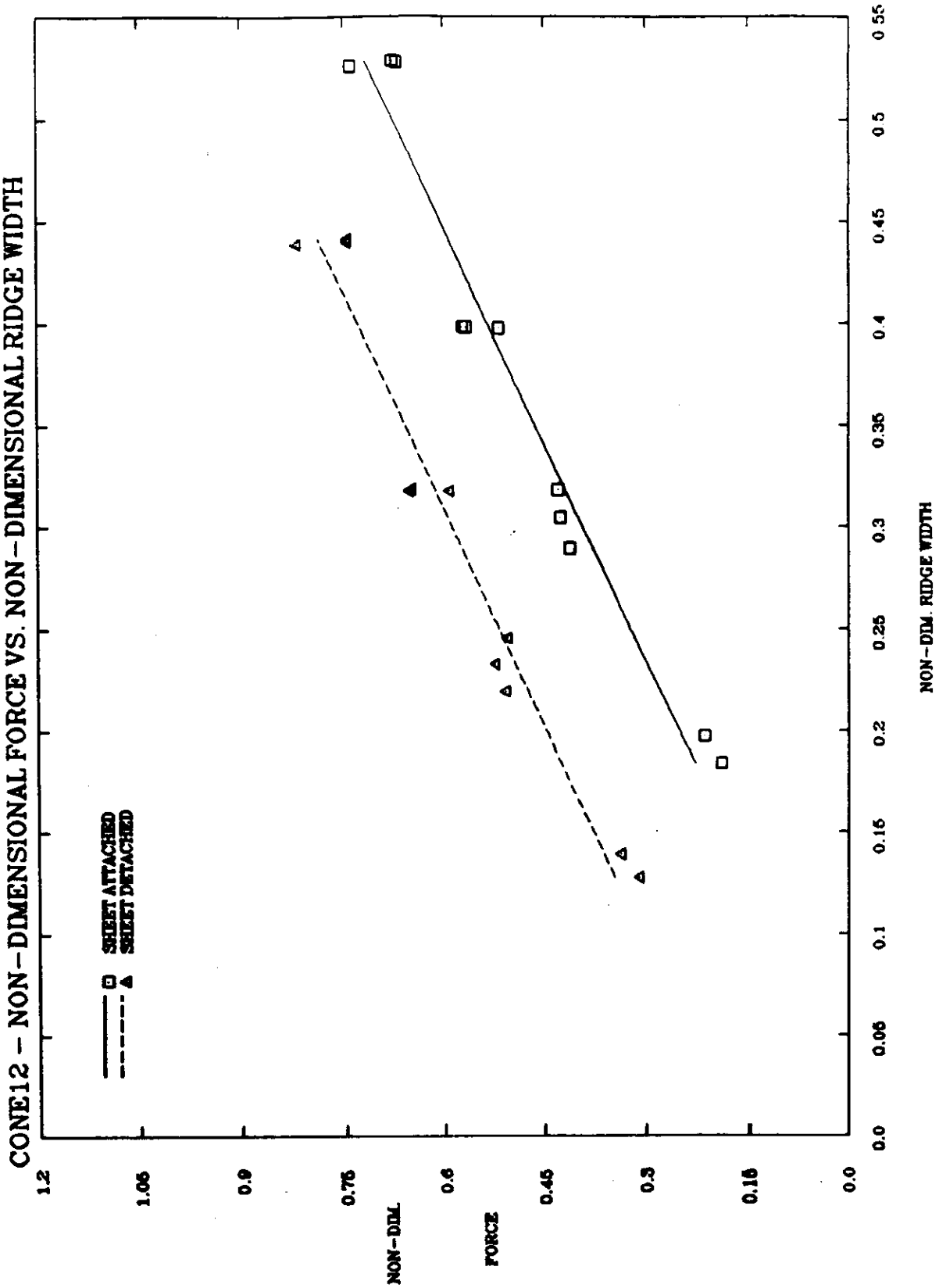
CONE12 - NON-DIMENSIONAL FORCE VS. NON-DIMENSIONAL RIDGE WIDTH
SHEET ATTACHED
SHEET DETACHED
NON-DIM. FORCE
NON-DIM. RIDGE WIDTH
1.2
1.05
0.9
0.75
0.6
0.45
0.3
0.15
0.0
0.0
0.05
0.1
0.15
0.2
0.25
0.3
0.35
0.4
0.45
0.5
0.55